Chinese Journal of Chemical Engineering 67 (2024) 58–67

Contents lists available at ScienceDirect

Chinese Journal of Chemical Engineering

journal homepage: www.elsevier.com/locate/CJChE

Full Length Article

Tungsten oxide/nitrogen-doped carbon nanotubes composite catalysts for enhanced redox kinetics in lithium–sulfur batteries

Deqing He [1], Zihao Xie [1], Qian Yang [1], Wei Wang [2], Chao Su [1,*]

[1] School of Energy and Power, Jiangsu University of Science and Technology, Zhenjiang 212100, China
[2] State Key Laboratory of Materials-Oriented Chemical Engineering, College of Chemical Engineering, Nanjing Tech University, Nanjing 211816, China

ARTICLE INFO

Article history:
Received 4 May 2023
Received in revised form
5 November 2023
Accepted 12 November 2023
Available online 21 December 2023

Keywords:
Li-S batteries
Composites
Ion diffusion channels
3D electron transport network
Redox kinetics

ABSTRACT

The sluggish redox kinetics of polysulfides in lithium–sulfur (Li–S) batteries are a significant obstacle to their widespread adoption as energy storage devices. However, recent studies have shown that tungsten oxide (WO_3) can facilitate the conversion kinetics of polysulfides in Li–S batteries. Herein, we fabricated host materials for sulfur using nitrogen-doped carbon nanotubes (N-CNTs) and WO_3. We used low-cost components and simple procedures to overcome the poor electrical conductivity that is a disadvantage of metal oxides. The composites of WO_3 and N-CNTs (WO_3/N-CNTs) create a stable framework structure, fast ion diffusion channels, and a 3D electron transport network during electrochemical reaction processes. As a result, the WO_3/N-CNT-Li_2S_6 cathode demonstrates high initial capacity (1162 $mA \cdot h \cdot g^{-1}$ at 0.5 C), excellent rate performance (618 $mA \cdot h \cdot g^{-1}$ at 5.5 C), and a low capacity decay rate (0.093% up to 600 cycles at 2 C). This work presents a novel approach for preparing tungsten oxide/carbon composite catalysts that facilitate the redox kinetics of polysulfide conversion.

1. Introduction

To achieve a sustainable future, it is widely believed that there is a pressing need to replace traditional energy sources. Lithium-ion batteries are widely appreciated as a green storage device with high energy density and a long cycle life [1]. However, their limitations in energy density and high material costs have prompted researchers to explore new energy storage systems that can meet the growing demand for high-performance batteries [2–4]. With their high energy density, low cost, and non-polluting cathode sulfur, Li–S batteries are considered a promising new energy storage device. Li–S batteries operate on a different principle than Li-ion batteries, where Li^+ moves between the anode and cathode during charge and discharge cycles. In Li–S batteries, sulfur undergoes a redox reaction with Li^+ to form lithium sulfides, resulting in high theoretical specific capacity [5–8]. Unfortunately, issues such as low cycle life, low sulfur utilization, and poor rate performance disturb the practicality and application of Li–S batteries [9–11]. To overcome these challenges, researchers are developing low-cost, highly efficient, and highly stable electrocatalysts for the cathode, such as porous carbon matrices, metal oxides, and conducting polymers, to improve the electrochemical reaction kinetics and stability of polysulfides. Thus, the incorporation of cathode host materials in Li–S batteries can enhance their electrochemical performance and contribute to the safety of the Li–S batteries [12,13].

Recent studies have concentrated on the design of metal oxide/carbon composite materials for use in Li–S batteries [14–17]. Sericin-derived carbon/Co_3O_4 hollow microspheres enhance sulfur cathode performance through polar chemisorption, physical encapsulation, and high conductivity. This approach shows promise for creating high-performance sulfur cathodes [18]. Another study has demonstrated that utilizing α-MoO_3 as cathode host materials for sulfur can alleviate the volume change caused by the electrochemical reaction of active sulfur and make more sulfur participate in electrochemical reactions, thus enhancing the energy storage characteristics of Li–S batteries [19].

Tungsten oxide, in particular, has shown great potential as a cathode host material in Li–S batteries due to its high electronic conductivity and ability to promote sulfur utilization [20–23]. It has been reported that a three-dimensional hierarchical structure made of reduced graphene and tungsten oxide framework catalyze the conversion of polysulfides, resulting in improved performance

* Corresponding author.
E-mail address: chao.su@just.edu.cn (C. Su).

https://doi.org/10.1016/j.cjche.2023.11.022
1004-9541/

of lithium-sulfur batteries [20]. Overall, the combination of metal oxide and carbon-based materials offers a promising strategy for overcoming the current issues faced by Li–S batteries, and tungsten oxide has shown particular potential as an effective metal oxide material for use in Li–S batteries. Overall, the combination of tungsten oxide and carbon-based materials represents a promising approach to improving the performance of Li–S batteries.

In this work, a novel material composed of nitrogen-doped carbon nanotubes embedded with tungsten oxide (WO_3/N-CNT) was investigated as a potential host material for sulfur in Li–S batteries. This material was found to have Li^+ diffusion tunnels and an integrated conductive structure, which improved the electrochemical performance of Li–S batteries. Additionally, the WO_3/N-CNT material was shown to have active sites with superior affinity and catalytic ability to polysulfides, resulting in improved cycle life and rate capability of Li–S batteries. The WO_3/N-CNT-Li_2S_6 cathode exhibited high initial discharge capacity (1162 $mA \cdot h \cdot g^{-1}$ at 0.5 C, 1 C = 1675 $mA \cdot h \cdot g^{-1}$), excellent rate performance (635 $mA \cdot h \cdot g^{-1}$ at 5.5 C), and good cycling stability (0.093% capacity decay per cycle after 600 cycles at 2 C). This study contributed valuable insights into the selection and design of functionalized WO_3-based cathode host materials in Li–S batteries.

2. Results and Discussion

The scheme presented in Fig. 1 illustrates the process of preparing WO_3/N-CNT composites using sodium tungstate, citric acid, and $C_{19}H_{42}BrN$ as raw materials. Carbon materials, such as carbon nanotubes (CNTs), are commonly employed as catalyst supports due to their excellent electronic conductivity and mechanical flexibility. In this scheme, sodium tungstate, citric acid, and $C_{19}H_{42}BrN$ are dissolved in an aqueous solution, leading to a three-component reaction that forms a white gel-like precursor. The precursor is then subjected to high-temperature annealing, resulting in the formation of the WO_3/N-CNT composite material in a single step. WO_3, as an oxide, possesses poor electronic conductivity, which hinders its efficient catalytic effect. To address this issue, it is combined with CNTs to facilitate electron transport within the electrode. However, carbon materials alone have a weak affinity for polysulfides, which can lead to the undesirable shuttling effect of polysulfides. To enhance the ability of CNTs to anchor polysulfides, nitrogen (N) elements are doped into the CNT structure. The incorporation of N into CNTs improves their interaction with polysulfides, effectively inhibiting the shuttling effect. Consequently, the combination of WO_3 and N-CNTs alleviates the

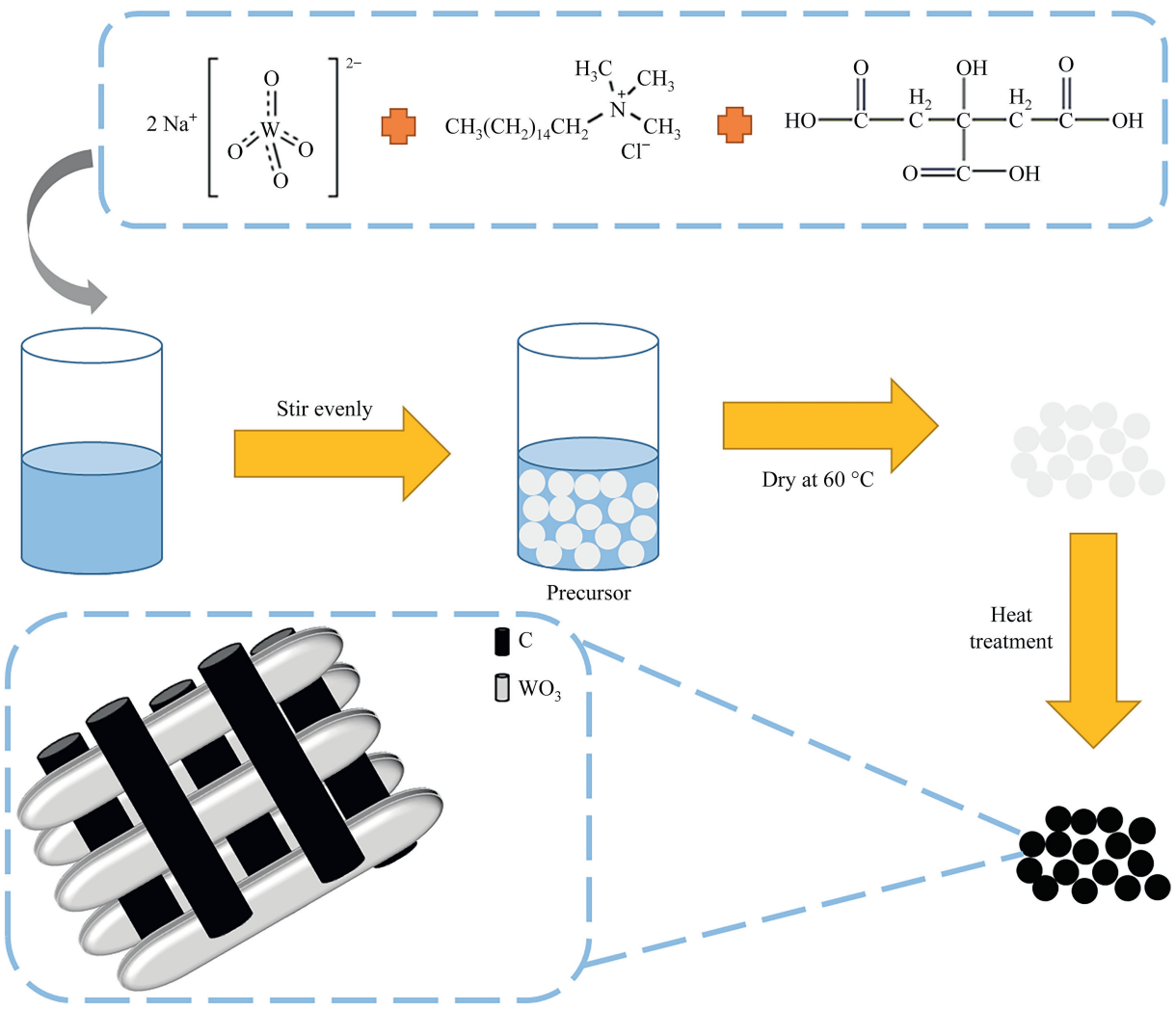

Fig. 1. (a) Illustration of synthetic process for the WO_3/N-CNT.

polysulfide shuttling effect and accelerates the conversion of polysulfides, thereby enhancing the electrochemical performance of Li–S batteries.

Fig. 2(a) shows the X-ray powder diffraction (XRD) pattern of WO_3/N-CNT, which exhibited main diffraction peaks that matched well with the characteristic peaks of WO_3 (JCPDS no. 46-1096), confirming the successful synthesis of WO_3. However, one broad diffraction peak was observed at 2θ of 24°, corresponding to the amorphous carbon material [24–26]. Since the carbon materials in WO_3/N-CNT are amorphous or nanocrystalline, little structural information can be obtained from XRD analysis. To investigate the heteroatoms that are doped in the carbon material and their chemical states, X-ray photoelectron spectroscopy (XPS) analysis was also performed. The full scan spectrum of XPS analysis is presented in Fig. 2(b), showing that the main composition elements of WO_3/N-CNT were O, N, C, and W. Deconvolution of the XPS C 1s spectra of WO_3/N-CNT revealed three peaks that could be attributed to the C–C, C–N, and C=O groups located at around 284.33 eV, 285.14 eV, and 288.05 eV, respectively (Fig. 2(c)) [27]. Additionally, the W 4f spectrum displayed two doublets of the W^{6+} ion at 38.2 and 36.1 eV, as well as the W^{5+} ion at 34.9 eV (Fig. 2(d)) [28]. Overall, XPS analysis provided insight into the chemical composition and bonding states of WO_3/N-CNT.

The morphology and structure of the N-CNT and WO_3/N-CNT were further investigated using scanning electron microscopy (SEM) and high-resolution transmission electron microscopy (HRTEM) techniques. Fig. 3(a), (b) and (c), (d) showed the low and high magnified SEM images of the N-CNT and WO_3/N-CNT, respectively. The N-CNT sample exhibited a porous structure with irregular shapes and sizes (Fig. 3(a), (b)). The specific surface area (38.8385 $m^2 \cdot g^{-1}$) and micropore volume (0.001442 $cm^3 \cdot g^{-1}$) of WO_3/N-CNT were determined through nitrogen adsorption-desorption experiments (Fig. S1 in Supplementary Material). The unsatisfactory specific surface area and pore volume of WO_3/N-CNT powder can be attributed to the introduction of WO_3 into N-CNT. However, this reduction is done intentionally to improve the powder's ability to adsorb and catalyze polysulfides in the cathode. By introducing WO_3, the cathode becomes more effective in capturing and reacting with polysulfides, which can enhance the performance of the Li–S batteries. In contrast, the WO_3/N-CNT sample exhibited a well-defined microsphere structure with a diameter of approximately 2 μm (Fig. 3(c), (d)). The excellent structure of the WO_3/N-CNT benefits from this precursor *via* a three-component reaction, which not only increases the number of sites available for the electrochemical reaction between sulfur and Li^+ but also facilitates faster diffusion of Li^+ by enhancing the effective contact area between the active material and the electrolyte. The WO_3/N-CNT microspheres were assembled by numerous WO_3 nanorods with a length of 500 nm and carbon nanotubes, forming a network-like structure. The topography of

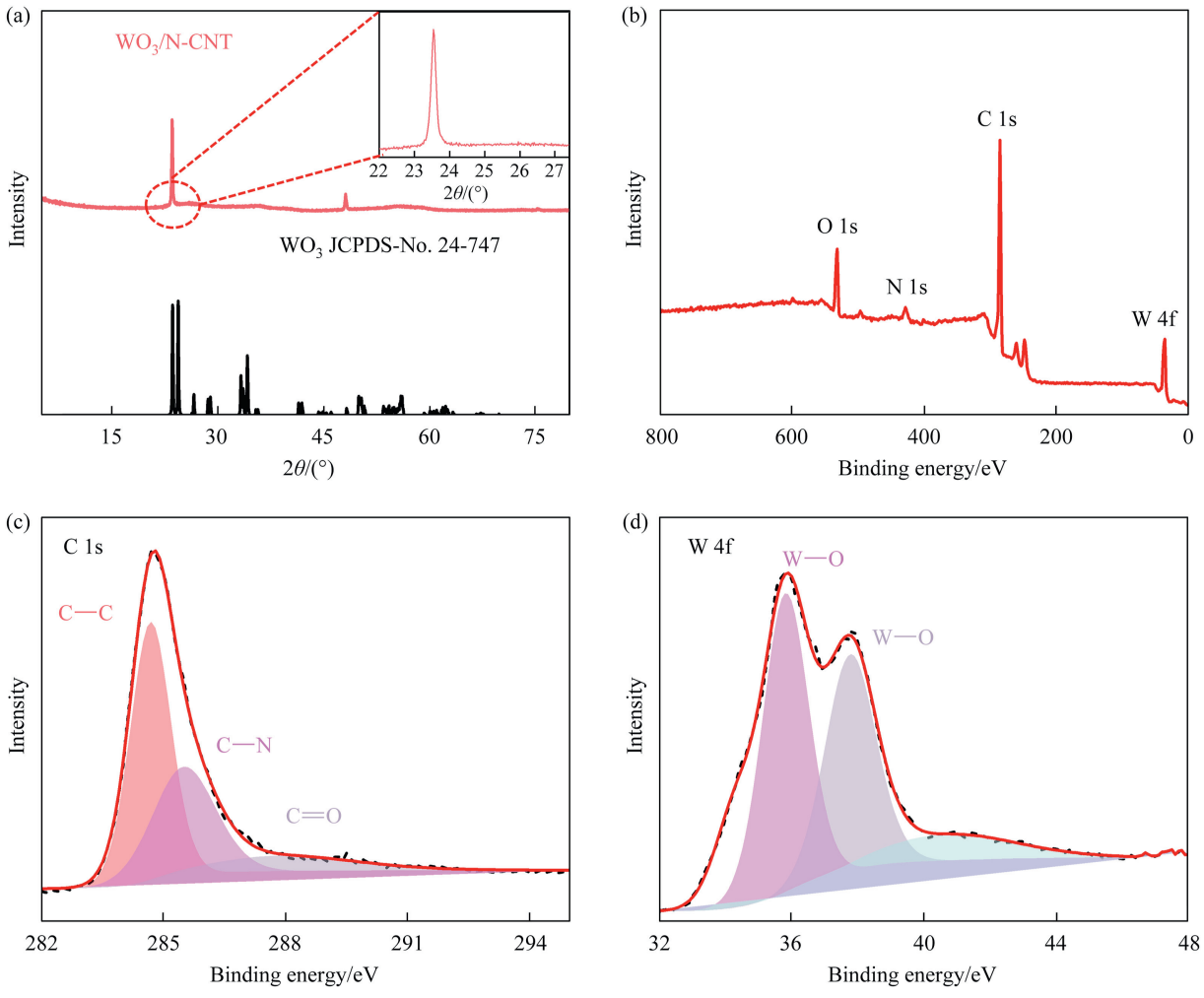

Fig. 2. (a) The XRD pattern and (b)–(d) the high-resolution XPS spectra for WO_3/N-CNT: (b) survey spectrum; (c) C 1s; (d) W 4f.

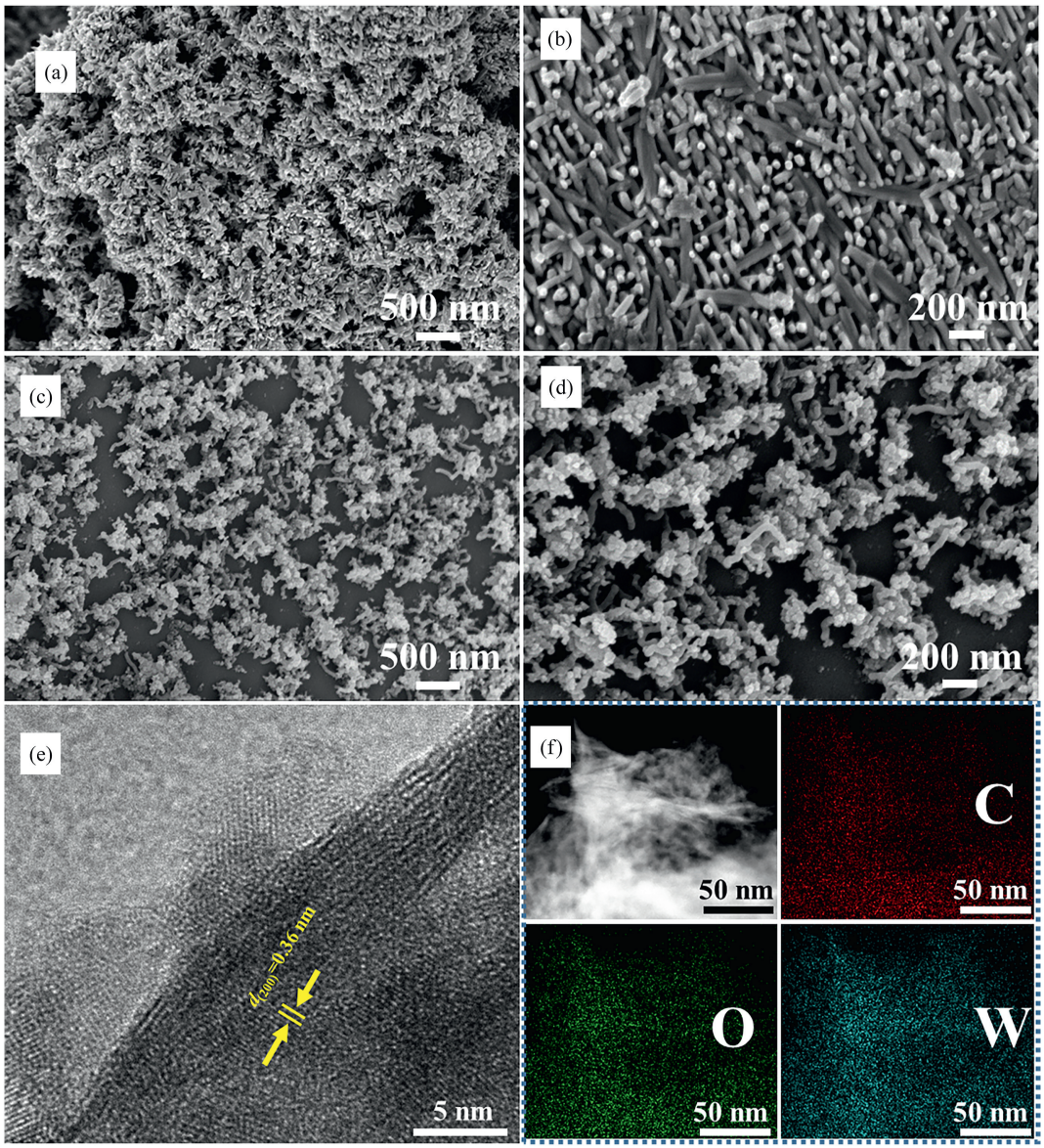

Fig. 3. FESEM images of (a), (b) WO_3/N-CNT and (c), (d) N-CNT. (e), (f) TEM image and corresponding elemental mappings of WO_3/N-CNT.

CNTs, derived from organic polymers, is comparable to that of WO_3/N-CNT, as shown in Fig. 3(c), (d). However, the presence of large aggregates in the CNT sample indicates poor dispersion. This may be attributed to the organic polymer derivation [29]. High-resolution transmission electron microscopy (HRTEM) images (Fig. 3(e)) revealed a lattice spacing of 0.36 nm, which corresponded to the WO_3 (2 0 0) plane. Moreover, energy dispersive X-ray spectroscopy (EDS) and elemental mappings suggested the coexistence and uniform distribution of O, W, and C on WO_3/N-CNT (Fig. 3(f)). The W element was mostly located in the core of the microspheres, while the C and O elements were uniformly distributed on the surface of the microspheres. The uniform distribution of elements in the WO_3/N-CNT structure was beneficial for electron and ion transfer and thus improved the electrochemical performance of Li–S batteries [30,31].

The strong chemical interactions between polysulfides and WO_3/N-CNT play a key role in suppressing the shuttling effect of polysulfides and enhancing the utilization of sulfur, resulting in improved electrochemical performance of Li–S batteries. To demonstrate the excellent polysulfide adsorption capability of WO_3/N-CNT, an adsorption test was conducted. Specifically, 100 mg of WO_3/N-CNT, WO_3, and N-CNT were added to three beakers containing 10 ml of diluted Li_2S_6 solution (5 mmol·L^{-1}). After 12 h of the adsorption test, the Li_2S_6 solutions containing WO_3/N-CNT, WO_3, and N-CNT showed a significant reduction in color intensity compared to the blank control experiment, indicating that all three materials are capable of effectively adsorbing polysulfides (Fig. 4(a)). After conducting the adsorption test, XPS was used to characterize the Li_2S_6-adsorbed WO_3/N-CNT. The Li 1s spectrum (shown in Fig. 4(b)) showed a peak at 56.35 eV corresponding to Li–N bonds and Li–O bonds. This peak indicates that Li_2S_6 is connected with WO_3 and N-CNT in the form of chemical bonds. Fig. 4(c)–(f) presents the scanning electron microscopy (SEM) images and energy-dispersive X-ray spectroscopy (EDS) analysis of the WO_3/N-CNT-Li_2S_6 cathode. These images and data allow for a direct visualization and evaluation of the distribution of Li_2S_6 on the surface of the WO_3/N-CNT cathode. Thanks to the strong affinity between WO_3/N-CNT and Li_2S_6, the agglomeration of Li_2S_6 particles

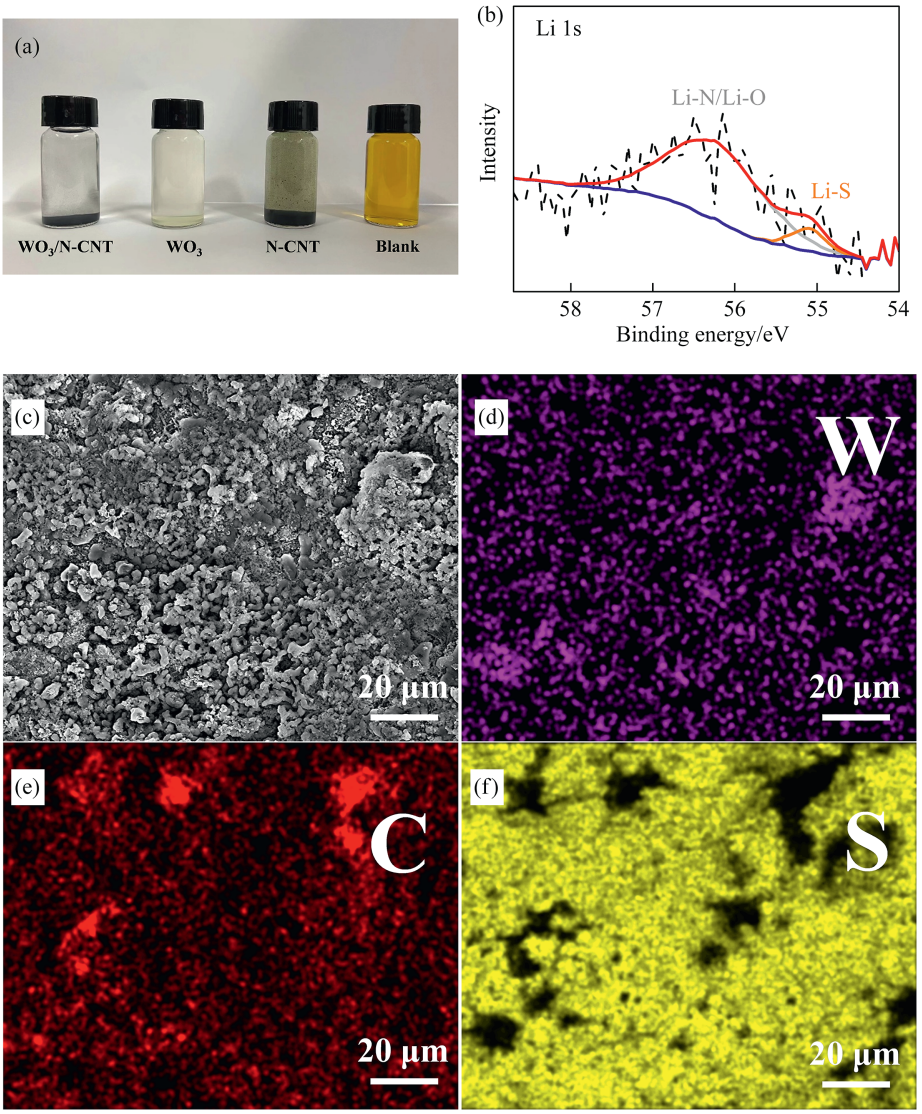

Fig. 4. (a) The optical photographs of the Li_2S_6 solution after exposure to the different materials. (b) XPS (Li 1s spectra) of WO_3/N-CNT after the adsorption test. (c–i) SEM images and corresponding elemental mappings of the WO_3/N-CNT- Li_2S_6 cathode.

on the electrode surface is prevented, resulting in the even deposition of Li_2S_6 on the cathode surface. The distribution of Li_2S_6 species on the cathode surface directly impacts the battery's overall performance. An even and well-dispersed distribution of Li_2S_6 ensures efficient utilization of active materials and facilitates better contact with the functional materials (WO_3/N-CNT or N-CNT). Optimizing the distribution of Li_2S_6 on the cathode surface through SEM analysis enhances the reaction kinetics of polysulfides, thereby improving the electrochemical performance of Li–S batteries.

The conversion rate of polysulfides in Li–S batteries can be effectively monitored by testing the deposition rate of Li_2S on the surfaces of different cathode materials. In this study, a constant current discharge was conducted at 0.05 C to learn about the precipitation phenomenon (Fig. 5(a) and (b)). The cut-off potential was set at 2.10 V, and the current was limited below 0.01 mA. The peak current of the WO_3/N-CNT cathode appeared earlier (at 12382 s) than that of the N-CNT cathode (at 16910 s), indicating that WO_3/N-CNT can efficiently reduce the nucleation overpotential of Li_2S and promote the precipitation of Li_2S [32]. To gain a deeper understanding of the kinetic mechanism, more detailed cyclic voltammetry (CV) analysis was conducted for the two cathode materials, and the results are presented in Fig. 5(c) and (d). In the cathodic scan, the two cathodic peaks at different potentials correspond to the two-step reduction reaction of elemental sulfur (S_8) to long-chain polysulfides (Li_2S_x, $4 \leq x \leq 8$) at the higher potential, followed by the reduction of polysulfides to Li_2S at the lower potential. Compared to the N-CNT cathode, the CV curve of the WO_3/N-CNT cathode exhibited higher current and smaller voltage polarization of the cathodic/anodic peaks, indicating improved redox reaction kinetics (Table S1). Upon further analysis of the CV curves for the two cathodes, it was confirmed that WO_3/N-CNT was superior to as cathode host materials [33]. The results are shown in Fig. S2(a), where the WO_3/N-CNT-Li_2S_6 cathode demonstrated remarkable advantages compared to the N-CNT-Li_2S_6 cathode. Notably, the CV curves of the WO_3/N-CNT-Li_2S_6 cathode than that of the N-CNT-Li_2S_6 cathode displayed a lower oxidation potential and a higher reduction potential at all three peaks. These results indicate a higher reaction reversibility and a lower polarization of polysulfides in the WO_3/N-CNT-Li_2S_6 cathode, making WO_3/N-CNT more suitable as cathode host material for Li–S batteries. Moreover, both WO_3/N-

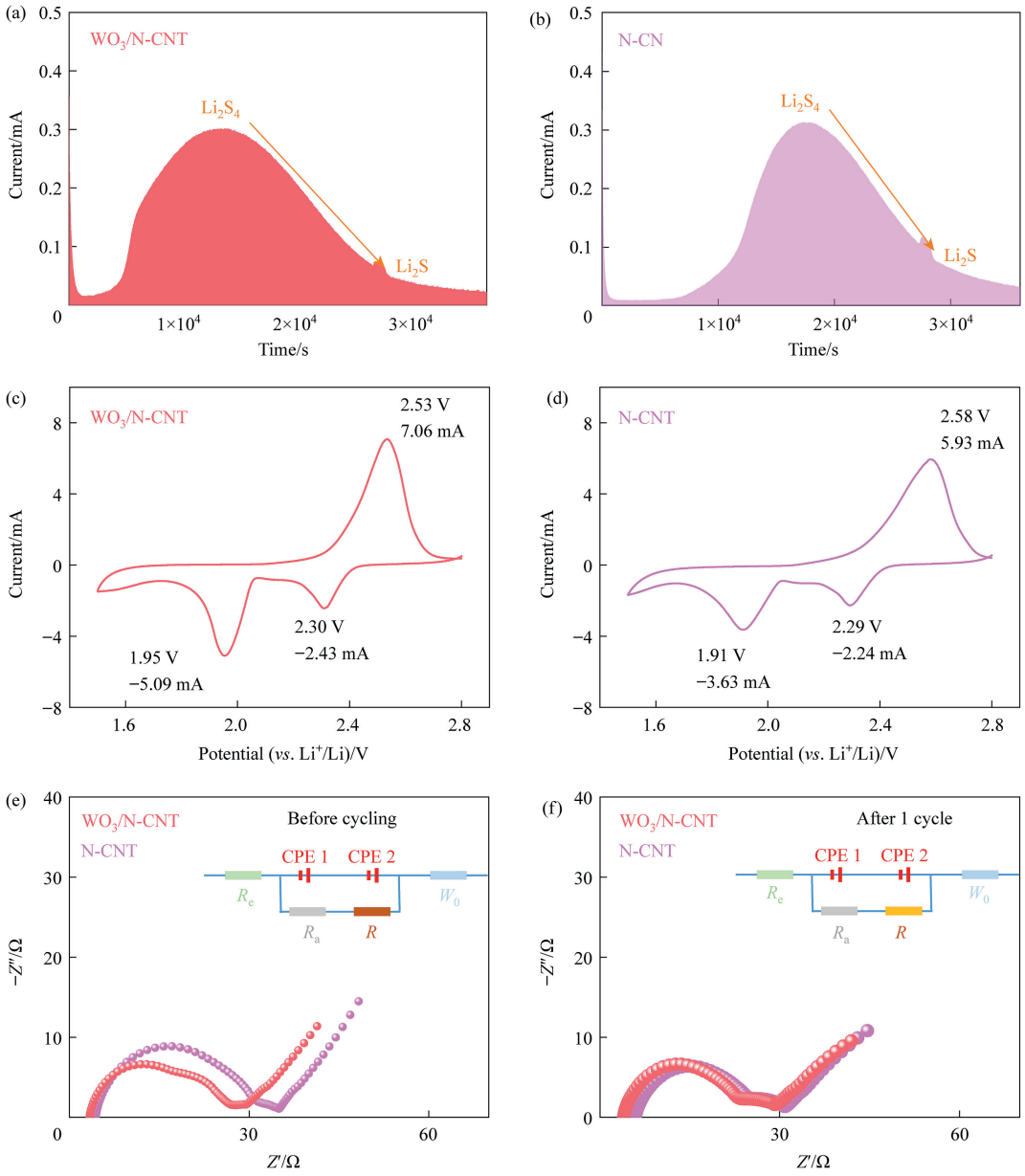

Fig. 5. Potentiostatic discharge profiles of Li–S batteries with (a) WO_3/N-CNT cathode and (b) N-CNT cathode; CV curve of (c) WO_3/N-CNT cathode and (d) N-CNT cathode; and EIS curves of (c) before cycling and (d) after 1 cycle.

CNT-Li_2S_6 cathodes exhibited sharper and higher current peaks, indicating a faster reduction rate of polysulfides. In contrast, polysulfides in the N-CNT-Li_2S_6 cathode had a slower reduction rate, as evidenced by a broad and low current peak at the second plateau. Overall, the results strongly support the use of WO_3/N-CNT as the cathode host material for Li–S batteries due to its superior properties. In Fig. S2(b), Gap 1 is between peak 1 and peak 3, and Gap 2 is between peak 1 and peak 2. The "Gap" values represent the difference in voltage values between specific peaks. From Fig. S2(b), it appears that the Gap 1 and Gap 2 values for the WO_3/N-CNT-Li_2S_6 cathode are lower (*i.e.* the voltage difference between peaks is smaller) than those of the N-CNT-Li_2S_6 cathode. This could indicate that the WO_3/N-CNT-Li_2S_6 cathode has better electrochemical reaction kinetics than the N-CNT-Li_2S_6 cathode. Furthermore, electrochemical impedance spectroscopy (EIS) was performed to study the impedance of the cathode materials. The EIS curves, shown in Fig. 5(e) and (f), were composed of several components, including R_e (the impedance resulting from the nature impedance of electrolyte resistance), R_a (the impedance attributable to charge transfer), $R_{Li_2S_6}$ (the impedance originating from the generation of Li_2S_6), and R_{S8} (the resistance of the formation of S_8) [34]. The R_a of WO_3/N-CNT after one cycle was found to be the lowest among the samples, suggesting that the "shuttle effect" was inhibited and the electron transfer was enhanced. After cycling, it becomes apparent that the resistance of both electrodes has significantly decreased. This can be attributed to the chemical activation process, which involves the dissolution and redistribution of active materials [35]. One notable change observed is the stark contrast in the EIS equivalent circuits before and after cycling. This disparity arises from the formation of S_8 as a result of the conversion of soluble Li_2S_6. In summary, the combination of various electrochemical techniques provided a comprehensive understanding of the superior electrochemical

performance of WO_3/N-CNT as a Li_2S_6 host material, which is attributed to the excellent structure of the WO_3/N-CNT composite and the synergistic interaction between WO_3 and N-CNT.

The imbalance between adsorption and catalytic conversion in Li–S batteries can lead to adverse consequences, impeding the subsequent "diffusion-conversion" process. To address this issue, the effectiveness of WO_3/N-CNT as a coordinator for regulating polysulfide capture/conversion and Li_2S decomposition was investigated. Li_2S_6 symmetric batteries were assembled, and the obtained CV curves are shown in Fig. 6(a)–(c) [36]. These tests were conducted to evaluate the catalytic ability of WO_3/N-CNT and N-CNT in reducing polysulfides in batteries containing Li_2S_6 solution. The results demonstrated that the WO_3/N-CNT electrode had the strongest response current compared to the other electrodes at various scan rates, indicating that WO_3/N-CNT possesses the highest catalytic activity in reducing polysulfides. A high Li ion diffusion rate is a reflection of excellent reaction kinetics of polysulfides and a reduced rate of Li dendrite formation, which indicates the improved cycle stability and rate performance of Li–S batteries [37,38]. A more detailed CV analysis of these electrodes is required to understand the kinetic mechanism involved. According to the classic Randles-Sevcik equation, the Li ion diffusion rate can be estimated by the following equation [39]:

$$I_p = 2.69 \times 10^5 n^{3/2} A D_{Li}^{1/2} V^{1/2} C_{Li}$$

To understand the Li ion diffusion rate on the surface of different materials, the classic Randles–Sevcik equation was used, where I_p represents the peak current, n represents the number of reaction electrons in the redox process (in this case, $n = 2$), A is the electrode area (1.13 cm^2 in this study), C_{Li} is the concentration of lithium ions, V is the scan rate, and D_{Li} is the diffusion coefficient of lithium ion. The absolute value of the slope observed in the I_p *vs.* $v^{0.5}$ plot in Fig. 6(d) serves as a measure of the diffusion coefficient (D_{Li}) of lithium ions. By analyzing the fitted slope values presented in this figure, it becomes apparent that the WO_3/N-CNT cathode exhibits a higher slope compared to the N-CNT cathode. This higher slope signifies a greater diffusion rate of lithium ions in the WO_3/N-CNT cathode. The observed enhancement in the diffusion rate of lithium ions in the WO_3/N-CNT cathode is indeed indicative of a more favorable reaction of polysulfides within the cathode. These characteristics are highly favorable in the context of Li–S batteries, as they contribute to enhanced cycle stability and rate capability [40]. However, further detailed electrochemical data analysis is needed to fully understand the kinetic mechanism underlying this improvement. To demonstrate the superiority of the high-temperature *in situ* synthesis of WO_3/N-CNT as the host material for Li–S batteries, a control experiment was conducted using a mixture of WO_3/N-CNT and N-CNT materials. The mass ratio of the WO_3/N-CNT composite material to the N-CNT material in the hybrid electrode was set at 1:0.5. This ratio was chosen to maintain consistency in the control experiment and to emphasize the effect of incorporating additional N-CNT composites on electrochemical performance. The results of the experiment revealed that the hybrid electrode exhibited the strongest response current, indicating that the introduction of WO_3 enhances the reaction kinetics of polysulfides (Fig. S3(a)). This observation suggests that the presence of homogeneously dispersed WO_3 in the hybrid electrode improves the electrochemical performance. The enhanced reaction kinetics can lead to more efficient utilization of sulfur species and improved battery performance. Furthermore, Fig. S3(b) illustrates that the ion diffusion coefficient (D_{Li}) of the composite electrode is not higher than that of the WO_3/N-CNT electrode. This could be attributed to the superior synthesis method employed for WO_3/N-

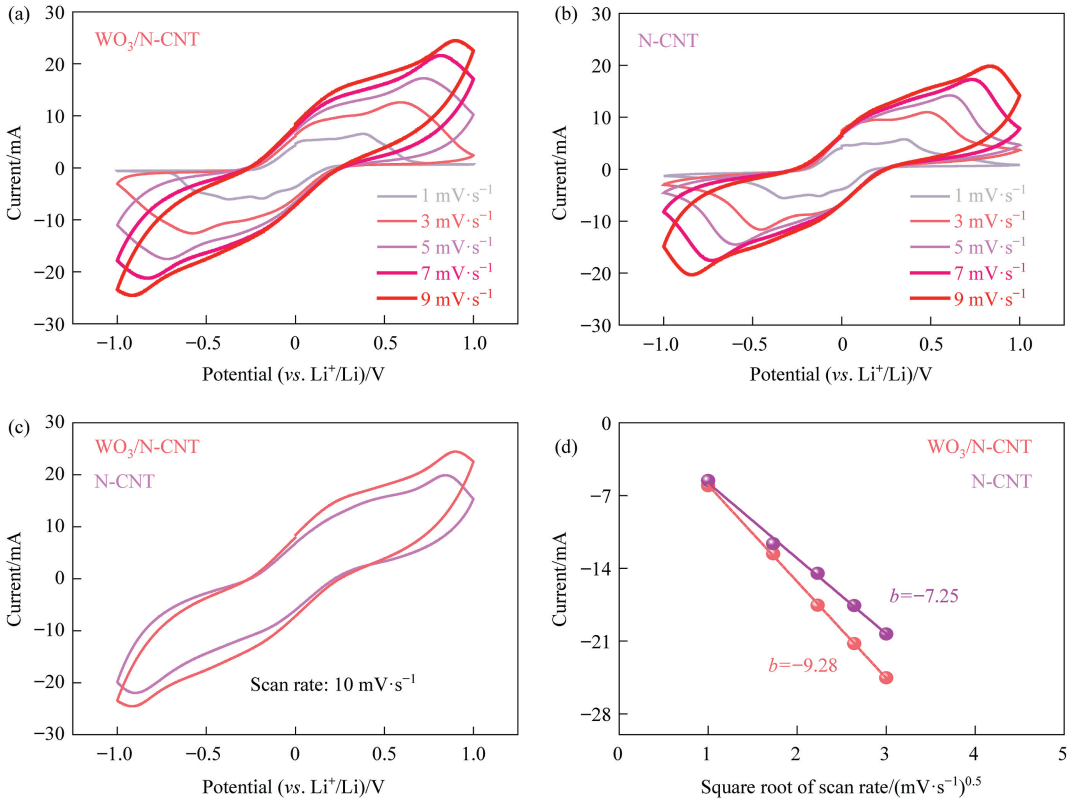

Fig. 6. (a–c) CV profiles of symmetric cells; (d) CV peak current of symmetric cells *versus* the square root of the scan rates.

CNT, which ensures a more uniform distribution of WO_3 and N-CNT within the electrode.

The use of WO_3/N-CNT as an efficient sulfur host enables the absorption of soluble polysulfides by strong chemical interaction, owing to their intrinsic polarity, while also promoting the redox kinetics of polysulfide conversion. The excellent conversion reaction kinetics of Li–S batteries can be observed through their outstanding rate performance and cycle stability, which are crucial parameters for their commercial application [41]. The rate performance tests were conducted to demonstrate the improved reaction kinetics of polysulfides when the WO_3/N-CNT cathode was used (Fig. 7(a)). The WO_3/N-CNT cathode (Li_2S_6 loading: 1 mg·cm^2) showed better rate performance and reversibility compared to the N-CNT cathode. The tests at different current rates (ranging from 1.1 C to 5.5 C) were carried out to evaluate their practicable application capability. The WO_3/N-CNT-Li_2S_6 cathode delivered discharge capacities of 944, 862, and 793 mA·h·g^{-1} when cycled at current rates of 1.1 C, 2.2 C, and 3.3 C, respectively, with a high coulombic efficiency of 98.0%. Even with the current rate increased to 4.4 C and 5.5 C, the WO_3/N-CNT-Li_2S_6 cathode still showed excellent reversible discharge capacities (711 and 618 mA·h·g^{-1}). In contrast, the N-CNT-Li_2S_6 cathode showed much lower capacities under the same rate conditions. The addition of WO_3/N-CNT accelerated the kinetics of polysulfides and suppressed the shuttle effect, thus restoring the high reversible capacity of the WO_3/N-CNT-Li_2S_6 cathode (952 mA·h·g^{-1}) when the current density returns to 1.1 C. The charge and discharge curves of these three cathodes at different rates (Fig. 7(b) and (c)) were analyzed to evaluate the capacity loss mechanism at high current density. The charge-discharge profile of the WO_3/N-CNT-Li_2S_6 cathode showed an obvious voltage plateau and a smaller voltage hysteresis compared to the N-CNT-Li_2S_6 cathode, demonstrating the kinetic improvement and polarization control achieved in the WO_3/N-CNT-based Li–S batteries *via* fast electrochemical reactions at elevated current density (Fig. 7(d)) [38].

The cyclic stability of traditional Li–S batteries is usually poor, resulting in a gradual decrease in their discharge capacity over multiple cycles. However, the WO_3/N-CNT-Li_2S_6 cathode exhibited remarkable capacity retention of 72% of its initial capacity even after 200 cycles, as shown in Fig. 8(a). Additionally, the conversion of polysulfides was evaluated for both electrodes. The Li–S batteries using the WO_3/N-CNT-Li_2S_6 cathode demonstrated significantly better cycling stability compared to the N-CNT-Li_2S_6 cathode, as shown in Fig. 8(b). In Fig. S4(a) and (b), the charge-discharge curves of Li–S batteries with different cathodes at the 10th, 100th, and 200th cycles are analyzed in order to understand why the electrochemical performance of WO_3/N-CNT-Li_2S_6 is superior to that of N-CNT-Li_2S_6. The galvanostatic discharge/charge curves of cathodes were compared at 1 C over 200 cycles. It was observed that the charge-discharge plateaus of both batteries gradually shortened and the polarization increased over time. However, the performance of WO_3/N-CNT-Li_2S_6 remained better than that of N-CNT-Li_2S_6 throughout the cycles. The results suggest that WO_3/N-CNT inhibits the "shuttle effect" more strongly than N-CNT. This means that more active materials are not deactivated in a short time, leading to better performance over the long term. The WO_3/N-CNT-Li_2S_6 cathode displayed good cyclic stability for up to 600 cycles at 1 C during the continuous discharge-charge tests, with a high capacity retention rate of 55% even after 600 cycles, whereas the N-CNT-Li_2S_6 cathode only retained 33% of its initial capacity after 230 cycles. The improved cycling stability of the WO_3/N-CNT-Li_2S_6 cathode is attributed to its improved reaction kinetics.

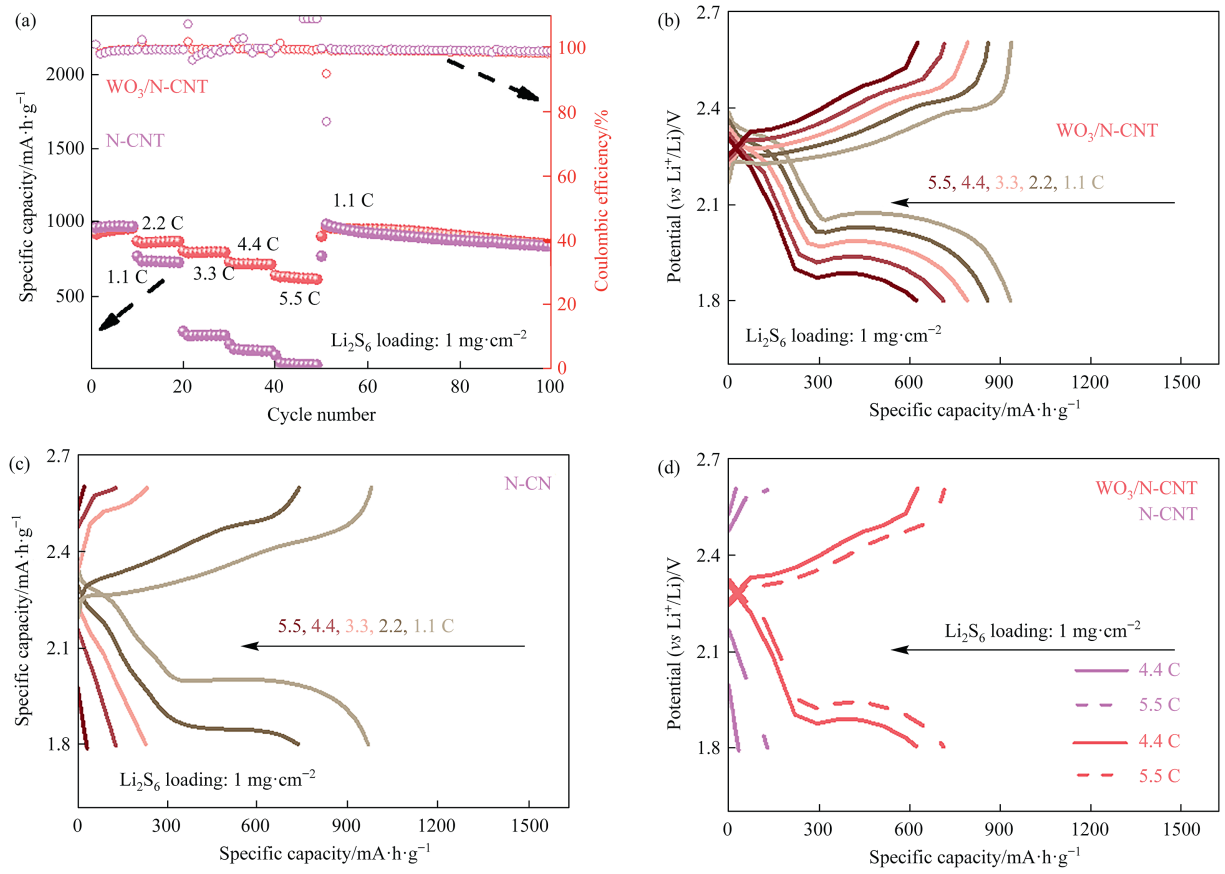

Fig. 7. (a) Rate performance and (b–c) corresponding charge/discharge curves; (d) charge/discharge curves of different electrodes at 4.4 and 5.5 C.

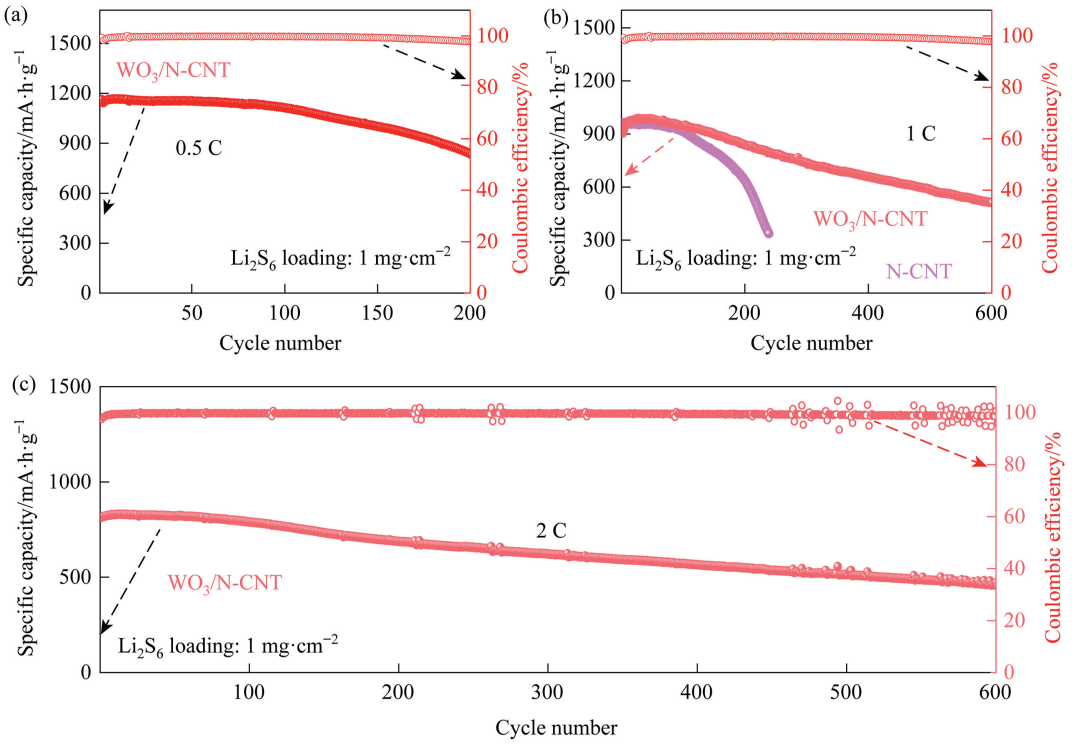

Fig. 8. Cycle performance at (a) 0.5, (b) 1 and (c) 2 C.

Notably, when the current density was increased to 2 C, the WO_3/N-CNT-Li_2S_6 cathode still maintained a discharge capacity of 455 mA·h·g^{-1} after 600 stable cycles, with a coulombic efficiency of 99% and an average capacity attenuation per cycle of only 0.093%, as shown in Fig. 8(c). There are two discharge platforms in the discharge process in the charge/discharge profiles at 2 C (Fig. S5). The first platform occurs at a voltage range of 2.30–2.40 V and corresponds to the formation of long-chain polysulfides. The second platform occurs at a lower voltage range of 2.10–2.15 V and corresponds to the transformation of long-chain polysulfides into short-chain polysulfides. This transformation is important because short-chain polysulfides are less soluble in the electrolyte and have lower migration rates, which can help improve the cycling stability and the overall performance of Li–S batteries. The WO_3/N-CNT-Li_2S_6 cathode exhibits a longer discharge plateau and a higher discharge platform voltage compared to the N-CNT-Li_2S_6 cathode, indicating that the WO_3/N-CNT-Li_2S_6 cathode has lower electrode polarization and improved electrochemical reaction kinetics during charge and discharge processes. This suggests that the addition of WO_3/N-CNT to the cathode can enhance the overall performance of the Li–S battery system.

3. Conclusions

In summary, this study demonstrates that WO_3/N-CNT composites can act as highly efficient Li_2S_6 host materials, offering superior electrochemical performance and enhanced catalytic activity in Li–S batteries. The WO_3/N-CNT-based cathode features abundant electron and ion transport channels, and its polar surface can provide anchoring sites for insoluble Li_2S and S. The experimental results reveal that WO_3/N-CNT can effectively catalyze the rapid conversion of polysulfides to Li_2S_2/Li_2S, leading to faster redox reaction kinetics and inhibition of the shuttle effect. Comparing to the N-CNT-Li_2S_6 cathode, the WO_3/N-CNT-Li_2S_6 cathode exhibits outstanding electrochemical performance with high specific capacitance, remarkable rate capability (618 mA·h·g^{-1} at 5.5 C), and long-term cycling stability (470 mA·h·g^{-1} after 600 cycles), benefiting from the synergistic interaction between WO_3 and N-CNT. This work not only provides new insights into the preparation of WO_3-based cathodes but also opens up new possibilities for the development of high-performance Li–S batteries.

Declaration of Interest

The authors declare that they have no known competing financial interests or personal relationships that could have appeared to influence the work reported in this paper.

Acknowledgements

This work is supported by the Open Project Program of the State Key Laboratory of Materials-Oriented Chemical Engineering (KL21-05). The authors acknowledge the support of the Instrumental Analysis Center, Jiangsu University of Science and Technology.

Supplementary Material

Supplementary data to this article can be found online at https://doi.org/10.1016/j.cjche.2023.11.022.

References

[1] J.L. Mao, J.Z. Miao, Y.Y. Lu, Z.M. Tong, Machine learning of materials design and state prediction for lithium ion batteries, *Chin. J. Chem. Eng.* 37 (2021) 1–11.
[2] L.Y. Hu, C.L. Dai, J.M. Lim, Y.M. Chen, X. Lian, M.Q. Wang, Y. Li, P.H. Xiao, G. Henkelman, M.W. Xu, A highly efficient double-hierarchical sulfur host for advanced lithium-sulfur batteries, *Chem. Sci.* 9 (3) (2017) 666–675.
[3] W.Q. Yao, J. Chen, L. Zhan, Y.L. Wang, S.B. Yang, Two-dimensional porous sandwich-like C/Si-graphene-Si/C nanosheets for superior lithium storage, *ACS Appl. Mater. Interfaces* 9 (45) (2017) 39371–39379.

[4] S.G. Chen, S.R. Jeong, S.W. Tao, Key materials and future perspective for aqueous rechargeable lithium-ion batteries, *Mater. Rep. Energy* 2 (2) (2022) 100096.
[5] S.H. Tian, Q. Zeng, G. Liu, J.J. Huang, X. Sun, D. Wang, H.C. Yang, Z. Liu, X.C. Mo, Z.X. Wang, K. Tao, S.L. Peng, Multi-dimensional composite frame as bifunctional catalytic medium for ultra-fast charging lithium-sulfur battery, *Nano Micro Lett.* 14 (1) (2022) 196.
[6] J. Scholz, B. Kayaalp, A.C. Juhl, D. Clemens, M. Fröba, S. Mascotto, Severe loss of confined sulfur in nanoporous carbon for Li–S batteries under wetting conditions, *ACS Energy Lett.* 3 (2) (2018) 387–392.
[7] X. Wu, N.N. Liu, B. Guan, Y. Qiu, M.X. Wang, J.H. Cheng, D. Tian, L.S. Fan, N.Q. Zhang, K.N. Sun, Redox mediator: A new strategy in designing cathode for prompting redox process of Li-S batteries, *Adv. Sci.* 6 (21) (2019) 1900958.
[8] C.Q. Shang, L.J. Cao, M.Y. Yang, Z.Y. Wang, M.C. Li, G.F. Zhou, X. Wang, Z.G. Lu, Freestanding Mo_2C-decorating N-doped carbon nanofibers as 3D current collector for ultra-stable Li-S batteries, *Energy Storage Mater.* 18 (2019) 375–381.
[9] Y. Hu, W. Chen, T.Y. Lei, Y. Jiao, J.W. Huang, A.J. Hu, C.H. Gong, C.Y. Yan, X.F. Wang, J. Xiong, Strategies toward high-loading lithium–sulfur battery, *Adv. Energy Mater.* 10 (17) (2020) 2000082.
[10] L. Huang, J.J. Li, B. Liu, Y.H. Li, S.H. Shen, S.J. Deng, C.W. Lu, W.K. Zhang, Y. Xia, G.X. Pan, X.L. Wang, Q.Q. Xiong, X.H. Xia, J.P. Tu, Electrode design for lithium–sulfur batteries: Problems and solutions, *Adv. Funct. Mater.* 30 (22) (2020) 1910375.
[11] C. Zhang, R.Y. Lyu, W. Lv, H. Li, W. Jiang, J. Li, S.C. Gu, G.M. Zhou, Z.J. Huang, Y. B. Zhang, J.Q. Wu, Q.H. Yang, F.Y. Kang, A lightweight 3D Cu nanowire network with phosphidation gradient as current collector for high-density nucleation and stable deposition of lithium, *Adv. Mater.* 31 (48) (2019) e1904991.
[12] Y.Y. Chang, J. Chen, Z. Zou, J. Li, C. Wu, Y.L. Jiang, Y. Chen, Q.X. Zeng, X.S. Wu, W. Sun, C.M. Li, Labyrinth maze-like long travel-reduction of sulfur and polysulfides in micropores of a spherical honeycomb carbon to greatly confine shuttle effects in lithium-sulfur batteries, *Mater. Rep. Energy* 2 (4) (2022) 100159.
[13] S.Y. Liu, Z.H. Song, X. Jin, R.Y. Mao, T.P. Zhang, F.Y. Hu, MXenes for metal-ion and metal-sulfur batteries: Synthesis, properties, and electrochemistry, *Mater. Rep. Energy* 2 (1) (2022) 100077.
[14] Q.Q. Huang, M.Q. Chen, Z. Su, L.Y. Tian, Y.Y. Zhang, D.H. Long, Rational cooperativity of nanospace confinement and rapid catalysis *via* hollow carbon nanospheres@Nb-based inorganics for high-rate Li-S batteries, *Chem. Eng. J.* 411 (2021) 128504.
[15] P.T. Xiao, F.X. Bu, G.H. Yang, Y. Zhang, Y.X. Xu, Integration of graphene, nano sulfur, and conducting polymer into compact, flexible lithium-sulfur battery cathodes with ultrahigh volumetric capacity and superior cycling stability for foldable devices, *Adv. Mater.* 29 (40) (2017) 1703324.
[16] Y.B. Zeng, F.Q. Chang, Q. Liu, L.Z. Duan, D.L. Li, H.C. Zhang, Recent advances and perspectives on the sources and detection of antibiotics in aquatic environments, *J. Anal. Methods Chem.* 2022 (2022) 5091181.
[17] M.H. Cheng, R. Yan, Z. Yang, X.F. Tao, T. Ma, S.J. Cao, F. Ran, S. Li, W. Yang, C. Cheng, Polysulfide catalytic materials for fast-kinetic metal-sulfur batteries: Principles and active centers, *Adv. Sci.* 9 (2) (2022) e2102217.
[18] J. Wu, Z.J. Pan, Y. Dai, T. Wang, H.P. Zhang, S. Yan, J.M. Xu, K.X. Song, Encapsulation of sulfur cathodes by sericin-derived carbon/Co_3O_4 hollow microspheres for the long-term cyclability of lithium-sulfur batteries, *J. Alloys Compd.* 823 (2020) 153912.
[19] P.H. Ji, B. Shang, Q.M. Peng, X.B. Hu, J.W. Wei, α-MoO_3 spheres as effective polysulfides adsorbent for high sulfur content cathode in lithium-sulfur batteries, *J. Power Sources* 400 (2018) 572–579.
[20] L.B. Ni, S.Q. Duan, H.Y. Zhang, J. Gu, G.J. Zhao, Z.X. Lv, G. Yang, Z.Y. Ma, Y. Liu, Y. S. Fu, Z. Wu, J. Xie, M. Chen, G.W. Diao, A 3D Graphene/WO_3 nanowire composite with enhanced capture and polysulfides conversion catalysis for high-performance Li–S batteries, *Carbon* 182 (2021) 335–347.
[21] X. Shi, I.Y. Choi, K. Zhang, J. Kwon, D.Y. Kim, J.K. Lee, S.H. Oh, J.K. Kim, J.H. Park, Efficient photoelectrochemical hydrogen production from bismuth vanadate-decorated tungsten trioxide helix nanostructures, *Nat. Commun.* 5 (2014) 4775.
[22] D. Chandra, K. Saito, T. Yui, M. Yagi, Crystallization of tungsten trioxide having small mesopores: Highly efficient photoanode for visible-light-driven water oxidation, *Angew. Chem. Int. Ed. Engl.* 52 (48) (2013) 12606–12609.
[23] X.Y. Lu, D.D. Wang, H.Q. Guo, P.C. Xiu, J.J. Chen, Y. Qin, H.M. Robin, C.Z. Xu, X.G. Zhang, X.L. Gu, Insights into depolymerization pathways and mechanism of alkali lignin over a $Ni_{1.2}$–ZrO_2/WO_3/γ-Al_2O_3 catalyst, *Chin. J. Chem. Eng.* 48 (2022) 191–201.
[24] Z.S. Chen, G.X. Zhang, Y.R. Wen, N. Chen, W.F. Chen, T. Regier, J. Dynes, Y. Zheng, S.H. Sun, Atomically dispersed Fe-co bimetallic catalysts for the promoted electroreduction of carbon dioxide, *Nano Micro Lett.* 14 (1) (2021) 25.
[25] Z.G. Liang, L.M. Zhang, H. Liu, J.P. Zeng, J.F. Zhou, H.J. Li, H. Xia, Formation of monodisperse carbon spheres with tunable size *via* triblock copolymer-assisted synthesis and their capacitor properties, *Nanosc. Res. Lett.* 14 (1) (2019) 124.
[26] X.M. Guo, J.F. Xie, J. Wang, S.Q. Sun, F. Zhang, F. Cao, Y.J. Liu, X.J. Zheng, J.H. Zhang, Q.H. Kong, Fabricating titanium dioxide/N-doped carbon nanofibers as advanced interlayer for improving cycling reversibility of lithium-sulfur batteries, *Chin. J. Chem. Eng.* 52 (2022) 88–94.
[27] H.T. Wang, X.Y. Qiu, W. Wang, L.P. Jiang, H.F. Liu, Iron sulfide nanoparticles embedded into a nitrogen and sulfur Co-doped carbon sphere as a highly active oxygen reduction electrocatalyst, *Front. Chem.* 7 (2019) 855.
[28] D.Q. He, X.J. Liu, X.R. Li, P.Z. Lyu, J.X. Chen, Z.H. Rao, Regulating the polysulfide redox kinetics for high-performance lithium-sulfur batteries through highly sulfiphilic $FeWO_4$ nanorods, *Chem. Eng. J.* 419 (2021) 129509.
[29] M.D. Sun, D.X. Pan, T.T. Ye, J. Gu, Y. Zhou, J. Wang, Ionic porous polyamide derived N-doped carbon towards highly selective electroreduction of CO_2, *Chin. J. Chem. Eng.* 55 (2023) 212–221.
[30] D.Q. He, J.B. Liu, B.X. Zhang, M. Wang, C.Z. Liu, Y.T. Huo, Z.H. Rao, Enhancing adsorption and catalytic activity of Marigold-like In_2S_3 in lithium-sulfur batteries by vacancy modification, *Chem. Eng. J.* 427 (2022) 131711.
[31] Y.B. Wang, Y. Jiang, Y.X. Zhao, X.L. Ge, Q. Lu, T. Zhang, D.S. Xie, M. Li, Y.F. Bu, Design strategies of perovskite nanofibers electrocatalysts for water splitting: a mini review, *Chem. Eng. J.* 451 (2023) 138710.
[32] L. Jiao, C. Zhang, C.N. Geng, S.C. Wu, H. Li, W. Lv, Y. Tao, Z.J. Chen, G.M. Zhou, J. Li, G.W. Ling, Y. Wan, Q.H. Yang, Capture and catalytic conversion of polysulfides by *in situ* built TiO_2-MXene heterostructures for lithium–sulfur batteries, *Adv. Energy Mater.* 9 (19) (2019) 1900219.
[33] Y.J. Zhong, X.M. Xu, Y. Liu, W. Wang, Z.P. Shao, Recent progress in metal–organic frameworks for lithium–sulfur batteries, *Polyhedron* 155 (2018) 464–484.
[34] L.M. Zhang, W.Q. Zhao, S.H. Yuan, F. Jiang, X.Q. Chen, Y. Yang, P. Ge, W. Sun, X. B. Ji, Engineering the morphology/porosity of oxygen-doped carbon for sulfur host as lithium-sulfur batteries, *J. Energy Chem.* 60 (2021) 531–545.
[35] L.X. Yuan, X.P. Qiu, L.Q. Chen, W.T. Zhu, New insight into the discharge process of sulfur cathode by electrochemical impedance spectroscopy, *J. Power Sources* 189 (1) (2009) 127–132.
[36] J.B. Li, Y.W. Chen, S.M. Zhang, W.F. Xie, S.M. Xu, G.R. Wang, M.F. Shao, Coordinating adsorption and catalytic activity of polysulfide on hierarchical integrated electrodes for high-performance flexible Li-S batteries, *ACS Appl. Mater. Interfaces* 12 (44) (2020) 49519–49529.
[37] W. Chen, T.Y. Lei, W.Q. Lv, Y. Hu, Y.C. Yan, Y. Jiao, W.D. He, Z.H. Li, C.L. Yan, J. Xiong, Atomic interlamellar ion path in high sulfur content lithium-montmorillonite host enables high-rate and stable lithium-sulfur battery, *Adv. Mater.* 30 (40) (2018) e1804084.
[38] P.Z. Lyu, X.J. Liu, J. Qu, J.T. Zhao, Y.T. Huo, Z.G. Qu, Z.H. Rao, Recent advances of thermal safety of lithium ion battery for energy storage, *Energy Storage Mater.* 31 (2020) 195–220.
[39] F. Yin, Q. Jin, H. Gao, X.T. Zhang, Z.G. Zhang, A strategy to achieve high loading and high energy density Li-S batteries, *J. Energy Chem.* 53 (2021) 340–346.
[40] L.D. Lin, F. Liang, K.Y. Zhang, H.Z. Mao, J. Yang, Y.T. Qian, Lithium phosphide/lithium chloride coating on lithium for advanced lithium metal anode, *J. Mater. Chem. A* 6 (32) (2018) 15859–15867.
[41] M.J. Shi, Z. Liu, S. Zhang, S.C. Liang, Y.T. Jiang, H. Bai, Z.M. Jiang, J. Chang, J. Feng, W.S. Chen, H.P. Yu, S.X. Liu, T. Wei, Z.J. Fan, A Mott–Schottky heterogeneous layer for Li–S batteries: Enabling both high stability and commercial-sulfur utilization, *Adv. Energy Mater.* 12 (14) (2022) 2103657.